Check for updates

Studies in Applied Mathematics

WILEY

STUDIES IN APPLIED MATHEMATICS

ORIGINAL ARTICLE OPEN ACCESS

Weakly Compressible Approximation of the Taylor–Green Vortex Solution

Matteo Antuono | Salvatore Marrone

Institute of Marine Engineering (INM), National Research Council of Italy (CNR), Roma, Italy

Correspondence: Matteo Antuono (matteo.antuono@cnr.it)

Received: 19 April 2024 | **Revised:** 15 October 2024 | **Accepted:** 5 November 2024

Funding: The work was partially supported by the Project BIO-EMBRACE, PRIN PNRR P202298P25—CUP B53D23026860001, financed by the European Union—Next Generation EU.

Keywords: analytical solutions | Taylor–Green vortex | weakly compressible flows

ABSTRACT

The Taylor–Green vortex represents an exact solution of the Navier–Stokes equations in $\mathbb{R}^2$. In this work, an approximation of this solution in two spatial dimensions is proposed for weakly compressible flows. These flows are characterized by small compressibility (or, equivalently, by a small Mach number) and are often employed in computational fluid dynamics to approximate the behaviour of incompressible Newtonian fluids. In this framework, the proposed solution is expected to be a useful benchmark for numerical solvers that implement the weakly compressibility approximation. To this end, some numerical examples are reported in the final section of this work.

1 | Introduction

Nowadays computational fluid dynamics (CFD) plays an important role in the modelling of many physical problems and phenomena in various fields of fluid mechanics. Several numerical approaches have been developed through the years, basing on different theoretical frameworks and spreading among a variety of numerical techniques, as, for example, finite difference methods, finite volume schemes, boundary element methods, particle schemes like smoothed particle hydrodynamics (SPH), moving particle semi-implicit (MPS) and many others. Aside from this, all numerical schemes need a constant and careful benchmarking stage to check their accuracy and robustness. In this context, the availability of analytical solutions (approximate or exact) is of crucial importance, since they allow inspecting some theoretical and practical aspects of the numerical implementation that would be difficult to tackle through generic applications.

This work inserts in the above line of research, aiming at providing an analytical solution for a class of numerical solvers that model weakly compressible flows to approximate the dynamics of incompressible fluids. The above technique allows some advantages in comparison to classic methods based on the hypothesis that the fluid is incompressible, since it leads to the implementation of explicit schemes that are easy to parallelize and do not need to solve large sparse linear systems (see, e.g., [1]). In turn, the availability of analytical solutions for weakly compressible flows is extremely limited and this induces many researchers to benchmark their schemes by means of solutions that hold true for incompressible fluid. Unfortunately, the validity of the latter approach becomes questionable when issues or incongruities arise during the benchmarking stage (see, e.g., [2–4]).

This is, in fact, the principal reason that motivates this work, where we propose a weakly compressible approximation in $\mathbb{R}^2$ of the well-known vortex solution by [5]. The celebrity of such a solution is due to its simplicity (the solution is defined over the two-dimensional plane with bi-periodic conditions and is expressed in form of elementary trigonometric functions) and to

This is an open access article under the terms of the Creative Commons Attribution License, which permits use, distribution and reproduction in any medium, provided the original work is properly cited.

© 2024 The Author(s). *Studies in Applied Mathematics* published by Wiley Periodicals LLC.

the possibility of inspecting the transition to turbulence for high Reynolds number flows (see, e.g., [6–8]). Despite its simple form, the Taylor–Green vortex hides some pitfalls when using weakly compressible solvers. In particular, the use of the incompressible solution as an initial condition causes the generation of spurious acoustic components during the flow evolution. For this reason many works in the literature do not provide time histories for local fields (i.e., pressure or velocity) but rather global quantities (e.g., global kinetic energy) which allow an easier benchmarking (see, e.g., [1, 9, 10] and many others). In this perspective, the availability of a weakly compressible correction to the Taylor–Green solution is expected to eliminate this issue. Incidentally, we observe that this solution is often referred to as Taylor–Green vortex, even though in the original work Taylor is the unique author while Taylor and Green appear in the subsequent paper (namely, [11]) that is devoted to the analysis of the early stages of the evolution of a viscous fluid from periodic three-dimensional initial conditions. An extension of the Taylor's solution to three-dimensional flows is described in [12]. Despite the procedure described in the paper formally applies to both two and three spatial dimensions, the derivation of the weakly compressible approximation of the three-dimensional solution of [12] is not considered here. In fact, this would require a considerable effort, because of the huge number of expressions and computations to handle, whereas its relevance for numerical applications would be relatively weak, since possible incongruities with respect to the incompressible solution would likely occur for high Reynolds numbers and, consequently, for very fine spatial resolutions, implying large computational costs.

This work is organized as follows: In Section 2 we describe the theoretical framework for attaining a weakly compressible approximation of an existing solution for an incompressible fluid, then in Section 3 we derive the approximate solution of the Taylor–Green vortex in two dimensions and, finally, in Section 4 we provide some numerical applications.

2 | Weak Compressibility Approximation

Let us consider the dimensionless Navier–Stokes equations for a viscous, compressible barotropic fluid:

$$\begin{cases} \dfrac{\partial \rho}{\partial t} + \nabla \cdot (\rho \boldsymbol{u}) = 0 \\ \dfrac{\partial \boldsymbol{u}}{\partial t} + \boldsymbol{u} \cdot \nabla \boldsymbol{u} = -\dfrac{\nabla p}{\rho} + \nu \Delta \boldsymbol{u} \qquad p = f(\rho). \end{cases} \tag{1}$$

Here, ρ is the fluid density, p is the pressure, $\boldsymbol{u}$ is the velocity field and ν is the dimensionless viscosity (namely, the inverse of the Reynolds number Re). Finally, f is a bijective function linking the pressure and density fields (called equation of state) and the symbols ∇ and Δ indicate the nabla and Laplacian operators, respectively. Hereinafter, we assume that the fluid is weakly compressible. This latter assumption corresponds to the condition $|dp/d\rho| \gg 1$ which, in fact, guarantees small density variations. As long as the above condition is satisfied, it is possible to linearize the equation of state as follows:

$$p = \frac{\rho - 1}{\epsilon}, \tag{2}$$

and consider the perturbation expansions below:

$$\rho = 1 + \epsilon \rho_1 + \epsilon^2 \rho_2 + \mathcal{O}(\epsilon^3), \qquad \boldsymbol{u} = \boldsymbol{u}_0 + \epsilon \boldsymbol{u}_1 + \mathcal{O}(\epsilon^2), \tag{3}$$

where $\epsilon = \mathrm{Ma}^2 \ll 1$ and Ma is the Mach number (that is the ratio between the reference fluid velocity and the sound speed). The above relations immediately imply:

$$p = \rho_1 + \epsilon \rho_2 + \mathcal{O}(\epsilon^2) = p_0 + \epsilon p_1 + \mathcal{O}(\epsilon^2), \tag{4}$$

that is, $p_n = \rho_{n+1}$ for $n \geq 0$. At the leading order, the system (1) gives:

$$\begin{cases} \nabla \cdot \boldsymbol{u}_0 = 0 \\ \dfrac{\partial \boldsymbol{u}_0}{\partial t} + \boldsymbol{u}_0 \cdot \nabla \boldsymbol{u}_0 = -\nabla p_0 + \nu \Delta \boldsymbol{u}_0, \end{cases} \tag{5}$$

which are the incompressible Navier-Stokes equations. Conversely, the first order is

$$\begin{cases} \dfrac{\partial p_0}{\partial t} + \boldsymbol{u}_0 \cdot \nabla p_0 + \nabla \cdot \boldsymbol{u}_1 = 0, \\ \dfrac{\partial \boldsymbol{u}_1}{\partial t} + \boldsymbol{u}_0 \cdot \nabla \boldsymbol{u}_1 + \boldsymbol{u}_1 \cdot \nabla \boldsymbol{u}_0 = -\nabla p_1 + \nabla\left(\dfrac{p_0^2}{2}\right) + \nu \Delta \boldsymbol{u}_1. \end{cases} \tag{6}$$

Introducing the vorticity field as below

$$\omega = \omega_0 + \epsilon \omega_1 + \mathcal{O}(\epsilon^2) \quad \text{where} \quad \omega_n = \nabla \times \boldsymbol{u}_n, \tag{7}$$

it is possible to derive an alternate form of the system (6), which will be useful in the analysis that follows. This reads:

$$\begin{cases} \dfrac{\partial p_0}{\partial t} + \boldsymbol{u}_0 \cdot \nabla p_0 + \nabla \cdot \boldsymbol{u}_1 = 0, \\ \dfrac{\partial \boldsymbol{u}_1}{\partial t} + \nabla(\boldsymbol{u}_0 \cdot \boldsymbol{u}_1) + \omega_0 \times \boldsymbol{u}_1 + \omega_1 \times \boldsymbol{u}_0 = -\nabla p_1 \\ \qquad + \nabla\left(\dfrac{p_0^2}{2}\right) + \nu \Delta \boldsymbol{u}_1. \end{cases} \tag{8}$$

Applying the curl operator to the momentum equation, we obtain the first-order vorticity equation:

$$\begin{aligned} &\tfrac{\partial \omega_1}{\partial t} + \nabla \cdot [\omega_0 \otimes \boldsymbol{u}_1 - \boldsymbol{u}_1 \otimes \omega_0] \\ &+ \nabla \cdot [\omega_1 \otimes \boldsymbol{u}_0 - \boldsymbol{u}_0 \otimes \omega_1] = \nu \Delta \omega_1, \end{aligned} \tag{9}$$

where the symbol $\otimes$ denotes the diadic product. In two dimensions, the vorticity field reduces to one component in the direction normal to the (x, y)-plane. Accordingly, we introduce the notation $\boldsymbol{\omega}_n = \omega_n \boldsymbol{e}_3$ where $\boldsymbol{e}_3$ is the unit vector normal to the (x, y)-plane. Hence, Equation (9) simplifies as follows:

$$\frac{\partial \omega_1}{\partial t} + \boldsymbol{u}_0 \cdot \nabla \omega_1 + \boldsymbol{u}_1 \cdot \nabla \omega_0 + \omega_0 \nabla \cdot \boldsymbol{u}_1 = \nu \Delta \omega_1. \tag{10}$$

The system (8), as well as Equation (10), have to be solved along with proper boundary conditions depending on the specific problem under consideration. In the next section, we apply the above perturbation expansion to the Taylor–Green vortex solution and provide the correct boundary conditions for its

14679590, 0, Downloaded from https://onlinelibrary.wiley.com/doi/10.1111/sapm.12792 by CNR GROUP 11 Istituto di Scienza dell', Wiley Online Library on [15/11/2024]. See the Terms and Conditions (https://onlinelibrary.wiley.com/terms-and-conditions) on Wiley Online Library for rules of use; OA articles are governed by the applicable Creative Commons License

weakly compressible correction. Part of the computations have been attained through the use of the software Mathematica [13].

3 | Weakly Compressible Taylor–Green Vortex

In the framework of the 2D incompressible Navier–Stokes equations, the Taylor–Green vortex solution reads:

$$u_0 = F\sin(2x)\cos(2y), \quad v_0 = -F\cos(2x)\sin(2y), \tag{11}$$

$$p_0 = \frac{F^2}{4}[\cos(4x)+\cos(4y)], \quad \omega_0 = 4F\sin(2x)\sin(2y), \tag{12}$$

where $F = \exp(-8\nu t)$. This corresponds to a tessellation of the $\mathbb{R}^2$-plane in bi-periodic squared patches with side length equal to unity. We consider the domain $\Omega = [0,\pi]\times[0,\pi]$ as a reference patch for the tessellation and observe that, as a consequence of this choice, the velocity flux is null between a patch and its neighbours. Similarly, we note that the vorticity field is null along $\partial\Omega$.

For the analysis that follows, it is also useful to recall the expression of the stream function associated to this solution, namely:

$$\psi_0 = \frac{F}{2}\sin(2x)\sin(2y) \tag{13}$$

recalling that in two dimensions $\boldsymbol{u}_0 = \nabla^\perp\psi_0$ where $\nabla^\perp = (\partial/\partial y, -\partial/\partial x)$ and $\omega_0 = -\Delta\psi_0$. We observe that the Taylor–Green solution belongs to the class of generalized Beltrami flows. This implies that the solution for the vorticity field solves the heat equation, while a constitutive relation holds true between the velocity and the vorticity field, namely:

$$\frac{\partial\omega_0}{\partial t} = \nu\Delta\omega_0 \qquad \text{and} \qquad \boldsymbol{u}_0\cdot\nabla\omega_0 = 0. \tag{14}$$

These results will be used later on to inspect some characteristics of the first-order correction.

To solve the system (8), we consider the classic Helmholtz decomposition of the velocity field into a gradient and a divergence-free component. In two spatial dimensions, this corresponds to introducing the potential ϕ_1 and the stream function ψ_1 as below:

$$\boldsymbol{u}_1 = \nabla\phi_1 + \nabla^\perp\psi_1. \tag{15}$$

The continuity equation immediately gives:

$$\Delta\phi_1 = -\left(\frac{\partial p_0}{\partial t} + \boldsymbol{u}_0\cdot\nabla p_0\right). \tag{16}$$

This equation is solved by imposing null Neumann conditions along $\partial\Omega$. The latter condition is chosen in order to maintain the same structure of the leading-order solution. Hence, we obtain the following solution for the potential ϕ_1:

$$\phi_1 = -\frac{\nu F^2}{4}[\cos(4x)+\cos(4y)] + \frac{F^3}{80}[\cos(6x)\cos(2y)-\cos(2x)\cos(6y)]. \tag{17}$$

In the following part, we distinguish the derivation of the viscous solution from the inviscid one. As shown in Section 3.2, this is motivated by the fact that the inviscid limit is non-trivial.

3.1 | Viscous Solution

Using the results of the previous section, the divergent-free component of the velocity field is achieved through the solution of the vorticity equation. Recalling that $\omega_1 = -\Delta\psi_1$ and substituting this expression in Equation (10), we find:

$$-\frac{\partial(\Delta\psi_1)}{\partial t} - \boldsymbol{u}_0\cdot\nabla(\Delta\psi_1) + \nabla^\perp\psi_1\cdot\nabla\omega_0 + \nabla\phi_1\cdot\nabla\omega_0 + \omega_0\Delta\phi_1 = -\nu\Delta^2\psi_1. \tag{18}$$

Accordingly to the leading-order solution, this equation is solved by requiring $\omega_1 = 0$ along $\partial\Omega$. For the sake of simplicity, it is convenient to rearrange the above equation as follows:

$$\mathcal{L}_{\psi_0}[\psi_1] = f, \tag{19}$$

where the operator $\mathcal{L}_{\psi_0}$ is given below:

$$\mathcal{L}_{\psi_0}[\psi_1] = -\frac{\partial(\Delta\psi_1)}{\partial t} - \nabla^\perp\psi_0\cdot\nabla(\Delta\psi_1) - \nabla^\perp\psi_1\cdot\nabla(\Delta\psi_0) + \nu\Delta^2\psi_1 \tag{20}$$

while the forcing term f is:

$$f = -[\nabla\phi_1\cdot\nabla\omega_0 + \omega_0\Delta\phi_1] = 8\nu F^3\sin(2x)\sin(2y) - 12\nu F^3[\sin(6x)\sin(2y)+\sin(2x)\sin(6y)] + \frac{7}{10}F^4[\sin(8x)\sin(4y)-\sin(4x)\sin(8y)]. \tag{21}$$

Since the incompressible solution depends on the composite variable $\tau = \nu t$, it is useful to decompose the linear operator in (20) as follows:

$$\mathcal{L}_{\psi_0}[\psi_1] = \nu\mathcal{A}[\psi_1] + \mathcal{B}_{\psi_0}[\psi_1], \tag{22}$$

where

$$\mathcal{A}[\psi_1] = -\frac{\partial(\Delta\psi_1)}{\partial\tau} + \Delta^2\psi_1$$
$$\mathcal{B}_{\psi_0}[\psi_1] = -\nabla^\perp\psi_0\cdot\nabla(\Delta\psi_1) - \nabla^\perp\psi_1\cdot\nabla(\Delta\psi_0). \tag{23}$$

Since ψ_0 represents a generalized Beltrami flow, it belongs to the kernel of both the operators $\mathcal{A}$ and $\mathcal{B}_{\psi_0}$ and, therefore, it belongs to the kernel of $\mathcal{L}_{\psi_0}$. This implies that the solution ψ_1 of Equation (19) is defined up to a component proportional to ψ_0. This issue will be addressed in the next section. Going back to the solution of Equation (19), the first and third components of the forcing term in Equation (21) can be eliminated by substituting:

$$\psi_1 = \widehat{\psi_1} - \frac{F^3}{16}\sin(2x)\sin(2y) + \frac{7F^3}{320}[\sin(6x)\sin(2y)+\sin(2x)\sin(6y)]. \tag{24}$$

14679590, 0, Downloaded from https://onlinelibrary.wiley.com/doi/10.1111/sapm.12792 by CNR GROUP 11 Istituto di Scienza dell', Wiley Online Library on [15/11/2024]. See the Terms and Conditions (https://onlinelibrary.wiley.com/terms-and-conditions) on Wiley Online Library for rules of use; OA articles are governed by the applicable Creative Commons License

This leads to:

$$\mathcal{L}_{\psi_0}[\hat{\psi}_1] = \hat{f}, \tag{25}$$

where

$$\hat{f} = 26\,\nu F^3[\sin(6x)\sin(2y) + \sin(2x)\sin(6y)]. \tag{26}$$

We observe that $\hat{f}$ is an eigenfunction of the operator $\mathcal{A}$ whereas it does not belong to the kernel of the operator $\mathcal{B}_{\psi_0}$. This implies that it can be only balanced by contributions of order $\mathcal{O}(\nu)$ in the solution of ψ_1. For high Reynolds number (namely for $\nu \ll 1$), these can be neglected so that the approximate solution satisfying $\omega_1 = 0$ along $\partial\Omega$ becomes:

$$\psi_1 = -\frac{F^3}{16}\sin(2x)\sin(2y) + \frac{7F^3}{320}[\sin(6x)\sin(2y) + \sin(2x)\sin(6y)] + \alpha\frac{F}{2}\sin(2x)\sin(2y) + \mathcal{O}(\nu), \tag{27}$$

where the last term represents a component proportional to ψ_0 belonging to the kernel of the operator $\mathcal{L}_{\psi_0}$ and α is a coefficient to be defined. Incidentally, we observe that $\nu = \mathcal{O}(\epsilon)$ is enough to guarantee that the above approximation is consistent with the perturbation expansion.

Before proceeding to the solution for the pressure field, we observe a further intriguing point. Let us focus on the first component of forcing term in Equation (21), namely $2\nu F^3\sin(2x)\sin(2y)$. This belongs to the kernel of $\mathcal{B}_{\psi_0}$ and it is an eigenfunction of the operator $\mathcal{A}$. Since this term and the operator $\mathcal{A}$ are both multiplied by ν, the corresponding contribution in the solution for ψ_1, namely $F^3\sin(2x)\sin(2y)/16$, is of order $\mathcal{O}(1)$. The fact that a forcing term of order $\mathcal{O}(\nu)$ gives back a term of order $\mathcal{O}(1)$ in the solution has interesting consequences in the evaluation of the inviscid limit, as addressed in Section 3.2.

From the knowledge of ϕ_1 and ψ_1 we obtain the solution for $\boldsymbol{u}_1$ according to the decomposition in (15). This reads:

$$u_1 = \nu F^2\sin(4x) - \frac{F^3}{16}\sin(2x)\cos(2y)[\cos(4x) - 5\cos(4y) + 5] + \alpha F\sin(2x)\cos(2y) + \mathcal{O}(\nu), \tag{28}$$

$$v_1 = \nu F^2\sin(4y) + \frac{F^3}{16}\cos(2x)\sin(2y)[-5\cos(4x) + \cos(4y) + 5] - \alpha F\cos(2x)\sin(2y) + \mathcal{O}(\nu). \tag{29}$$

The last step is, therefore, the solution for p_1. Incidentally, we observe that mass conservation implies that the average of the pressure field over Ω is zero, that is:

$$\int_0^\pi dx\int_0^\pi \rho dy = \pi^2 \;\Rightarrow\; \int_0^\pi dx\int_0^\pi \rho_2\,dy = \int_0^\pi dx\int_0^\pi p_1 dy = 0. \tag{30}$$

The solution for p_1 is obtained by decomposing the momentum equation (8) in its gradient and null-divergence components, that is:

$$\nabla\left[\frac{\partial\phi_1}{\partial t} + \boldsymbol{u}_0\cdot\boldsymbol{u}_1 + p_1 - \frac{p_0^2}{2} - \nu\Delta\phi_1\right] + \boldsymbol{\omega}_0\times\boldsymbol{u}_1 + \boldsymbol{\omega}_1\times\boldsymbol{u}_0 = \nabla^\perp\left[-\frac{\partial\psi_1}{\partial t} + \nu\Delta\psi_1\right]. \tag{31}$$

Applying the divergence operator, we find:

$$\Delta\chi = -\nabla\cdot[\boldsymbol{\omega}_0\times\boldsymbol{u}_1 + \boldsymbol{\omega}_1\times\boldsymbol{u}_0], \tag{32}$$

where

$$\chi = \frac{\partial\phi_1}{\partial t} + \boldsymbol{u}_0\cdot\boldsymbol{u}_1 + p_1 - \frac{p_0^2}{2} - \nu\Delta\phi_1 + H_1, \tag{33}$$

and $H_1 = H_1(t)$ is a function of time which is used to impose the mass conservation according to Equation (30). Since the solution for ψ_1 is accurate up to $\mathcal{O}(\nu)$, the same truncation is applied to the forcing term of the Poisson equation, leading to:

$$\begin{aligned}&-\nabla\cdot[\boldsymbol{\omega}_0\times\boldsymbol{u}_1 + \boldsymbol{\omega}_1\times\boldsymbol{u}_0]\\ &= \frac{3}{4}F^4[\cos(4x) + \cos(4y) - 4\cos(8x) - 4\cos(8y)\\ &- 4\cos(4x)\cos(4y) + 5\cos(8x)\cos(4y) + 5\cos(4x)\cos(8y)]\\ &+ 8\alpha F^2[-\cos(4x) - \cos(4y) + 2\cos(4x)\cos(4y)] + \mathcal{O}(\nu).\end{aligned} \tag{34}$$

The corresponding solution of the Poisson equation for χ is:

$$\chi = \frac{3}{64}F^4[-\cos(4x) - \cos(4y) + \cos(8x) + \cos(8y) + 2\cos(4x)\cos(4y) - \cos(8x)\cos(4y) - \cos(4x)\cos(8y)] + \alpha\frac{F^2}{2}[\cos(4x) + \cos(4y) - \cos(4x)\cos(4y)] + \mathcal{O}(\nu). \tag{35}$$

Finally, extracting the component p_1 from χ, substituting the leading orders of the remaining solutions and imposing the mass conservation according to (30), we find:

$$p_1 = \frac{F^4}{64}[-5\cos(4x) - 5\cos(4y) + \cos(8x) + \cos(8y) + 12\cos(4x)\cos(4y) - \cos(8x)\cos(4y) - \cos(4x)\cos(8y)] + \alpha\frac{F^2}{2}[\cos(4x) + \cos(4y) - \cos(4x)\cos(4y)] + \mathcal{O}(\nu). \tag{36}$$

Note that the above solution satisfies the condition $\partial p/\partial n = 0$ along $\partial\Omega$, accordingly to the leading-order solution p_0. A discussion on the choice of the parameter α is postponed to the following section.

Finally, we observe that the solution obtained in the present section satisfies the continuity equation exactly, while it approximates the momentum equation up to the order $\mathcal{O}(\nu)$. As a consequence of this approach, the gradient component of the velocity field is solved exactly, whereas the rotational part and the solution of the pressure field are solved up to the order $\mathcal{O}(\nu)$.

14679590, 0, Downloaded from https://onlinelibrary.wiley.com/doi/10.1111/sapm.12792 by CNR GROUP 11 Istituto di Scienza dell', Wiley Online Library on [15/11/2024]. See the Terms and Conditions (https://onlinelibrary.wiley.com/terms-and-conditions) on Wiley Online Library for rules of use; OA articles are governed by the applicable Creative Commons License

3.2 | Inviscid Solution and Consistency of the Inviscid Limit

This case is of interest because the inviscid solution (namely, the solution obtained by assuming $\nu = 0$) cannot be obtained straightforwardly as the limit for $\nu \to 0$ of the solution ψ_1 described in the previous section. As shown later, to make the inviscid limit consistent with the inviscid solution, we need to consider a proper contribution proportional to ψ_0.

For the incompressible case, the inviscid solution coincides with the inviscid limit and gives a steady solution with $F(\nu = 0) = F_0 = 1$. On the contrary, for the inviscid weakly compressible solution, we have to discriminate between the gradient field and the rotational part of the velocity field. The inviscid solution for the gradient field, hereinafter ϕ_1^*, is obtained immediately by applying the inviscid limit $\nu \to 0$ to Equation (17). We obtain:

$$\lim_{\nu\to 0} \phi_1 = \phi_1^* = \frac{F_0^3}{80}[\cos(6x)\,\cos(2y) - \cos(2x)\,\cos(6y)]. \quad (37)$$

On the contrary, the above limit does not hold true for the expression for ψ_1 in (27), unless we consider a component proportional to ψ_0 in the inviscid solution. This is caused by the disappearance of the first component in the forcing term in (21) (i.e., the term of order $\mathcal{O}(\nu)$ giving a contribution of order $\mathcal{O}(1)$ in the solution). The correct inviscid solution for the rotational field, denoted by ψ_1^*, is obtained by solving the problem:

$$\mathcal{B}_{\psi_0}\left[\psi_1^*\right] = \frac{7}{10}F_0^4[\sin(8x)\sin(4y) - \sin(4x)\sin(8y)], \quad (38)$$

which has the following exact solution:

$$\psi_1^* = \frac{7F_0^3}{320}[\sin(6x)\sin(2y) + \sin(2x)\sin(6y)] + \beta\frac{F_0}{2}\sin(2x)\sin(2y), \quad (39)$$

where the last component belongs to the kernel of $\mathcal{B}_{\psi_0}$ and β is a coefficient to be defined. Now, imposing the consistency with the inviscid limit, namely:

$$\lim_{\nu\to 0} \psi_1 = \psi_1^*, \quad (40)$$

we find the following relation between α and β:

$$\beta = \alpha - \frac{F_0^2}{8}. \quad (41)$$

For a viscous fluid, we assume that the component proportional to the incompressible solution is normalized to unity. This implies that $\alpha = 0$ is used hereinafter. Incidentally, we observe that the solution of the inviscid problem is exact. For this case, the fields p_0, p_1 and ω_0, ω_1 are displayed in Figure 1.

3.3 | Summary of the Analytical Results

For the reader's convenience, in this section, we summarize the results obtained so far for the weakly compressible correction. The potential and stream functions are:

$$\phi_1 = -\frac{\nu F^2}{4}[\cos(4x) + \cos(4y)] + \frac{F^3}{80}[\cos(6x)\cos(2y) - \cos(2x)\cos(6y)], \quad (42)$$

$$\psi_1 = -\frac{F^3}{16}\sin(2x)\sin(2y) + \frac{7F^3}{320}[\sin(6x)\sin(2y) + \sin(2x)\sin(6y)] + \mathcal{O}(\nu), \quad (43)$$

where $F = \exp(-8\nu t)$. Accordingly, the components of the velocity field are:

$$u_1 = \nu F^2\sin(4x) - \frac{F^3}{16}\sin(2x)\cos(2y)[\cos(4x) - 5\cos(4y) + 5] + \mathcal{O}(\nu), \quad (44)$$

$$v_1 = \nu F^2\sin(4y) + \frac{F^3}{16}\cos(2x)\sin(2y)[-5\cos(4x) + \cos(4y) + 5] + \mathcal{O}(\nu), \quad (45)$$

while the vorticity field reads:

$$\omega_1 = \frac{F^3}{4}\sin(2x)\sin(2y)[5 + 7\cos(4x) + 7\cos(4y)] + \mathcal{O}(\nu). \quad (46)$$

Finally, the pressure field is:

$$p_1 = \frac{F^4}{64}[-5\cos(4x) - 5\cos(4y) + \cos(8x) + \cos(8y) + 12\cos(4x)\cos(4y) - \cos(8x)\cos(4y) - \cos(4x)\cos(8y)] + \mathcal{O}(\nu). \quad (47)$$

According to the discussion of Section 3.2, the inviscid solution is attained straightforwardly by taking the limit $\nu \to 0$ of the expressions above. For the sake of the numerical implementation, we also include the expressions of the analytical solution in the domain $\Omega = [0,1]\times[0,1]$. These read:

$$\phi_1 = -\frac{\nu F^2}{4}[\cos(4\pi x) + \cos(4\pi y)] + \frac{F^3}{80\pi}[\cos(6\pi x)\cos(2\pi y) - \cos(2\pi x)\cos(6\pi y)], \quad (48)$$

$$\psi_1 = -\frac{F^3}{16\pi}\sin(2\pi x)\sin(2\pi y) + \frac{7F^3}{320\pi}[\sin(6\pi x)\sin(2\pi y) + \sin(2\pi x)\sin(6\pi y)] + \mathcal{O}(\nu), \quad (49)$$

$$u_1 = \nu\pi F^2\sin(4\pi x) - \frac{F^3}{16}\sin(2\pi x)\cos(2\pi y)$$

14679590, 0, Downloaded from https://onlinelibrary.wiley.com/doi/10.1111/sapm.12792 by CNR GROUP 11 Istituto di Scienza dell', Wiley Online Library on [15/11/2024]. See the Terms and Conditions (https://onlinelibrary.wiley.com/terms-and-conditions) on Wiley Online Library for rules of use; OA articles are governed by the applicable Creative Commons License

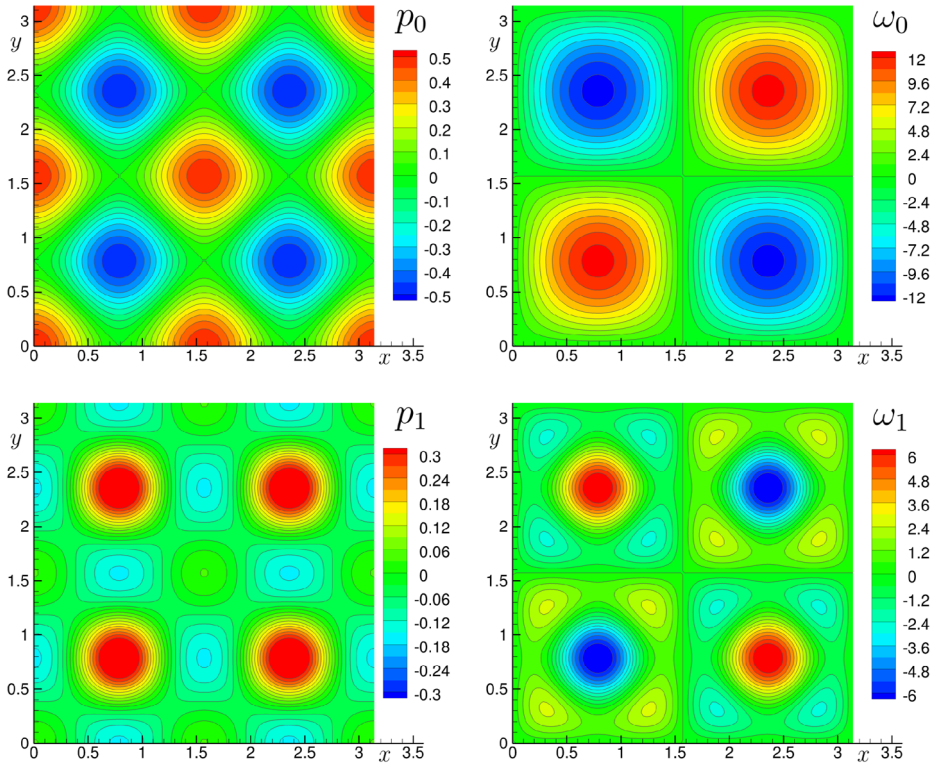

FIGURE 1 | Inviscid solution. Top panels: the Taylor–Green solution for the pressure (left) and vorticity (right) fields. Bottom panels: the first-order weakly compressible correction for the pressure (left) and vorticity (right) fields.

$$[\cos(4\pi x) - 5\cos(4\pi y) + 5] + \mathcal{O}(\nu), \tag{50}$$

$$v_1 = \nu\pi F^2 \sin(4\pi y) + \frac{F^3}{16}\cos(2\pi x)\sin(2\pi y)$$
$$[-5\cos(4\pi x) + \cos(4\pi y) + 5] + \mathcal{O}(\nu), \tag{51}$$

where $F = \exp(-8\pi^2\nu t)$. Finally, the vorticity and pressure fields are:

$$\omega_1 = \frac{\pi F^3}{4}\sin(2\pi x)\sin(2\pi y)[5 + 7\cos(4\pi x) + 7\cos(4\pi y)] + \mathcal{O}(\nu). \tag{52}$$

$$p_1 = \frac{F^4}{64}[-5\cos(4\pi x) - 5\cos(4\pi y) + \cos(8\pi x) + \cos(8\pi y) + 12\cos(4\pi x)\cos(4\pi y) - \cos(8\pi x)\cos(4\pi y) - \cos(4\pi x)\cos(8\pi y)] + \mathcal{O}(\nu). \tag{53}$$

4 | Applications

In this section, we consider some numerical applications that show the benefits of using the proposed weakly compressible correction to the Taylor–Green solution.

The numerical domain is $\Omega = [0, L] \times [0, L]$ where $L = 1$, and periodic boundary conditions are imposed along $\partial\Omega$. The reference velocity for the numerical simulations is $U = \max_\Omega(u_0) = \max_\Omega(v_0)$ at $t = 0$. We consider the Arbitray–Lagragian–Eulerian solver described in [14] which allows simulations in both Eulerian and Lagrangian frameworks. Such a solver belongs to the class of weakly compressible smoothed particle hydrodynamics (WC-SPH) schemes, that is, those SPH solvers that implement the weak-compressibility assumption to approximate incompressible flows. These kind of solvers rely on the mollification of the differential operators through proper kernel functions. In particular, we used a C2 Wendland kernel [15] with radius $R = 6\Delta x$ where Δx is the characteristic size of the spatial discretization (for more details, the reader is referred to [14]). All the simulations reported hereinafter are achieved by using a spatial resolution that ensures that the numerical outputs are close to convergence (namely, that negligible changes occur by increasing the resolution any further).

We first consider the case of an inviscid weakly compressible flow in an Eulerian framework. The adopted spatial discretization is $L/\Delta x = 200$. Figure 2 displays the evolution of the relative error of the pressure field measured at $\boldsymbol{x} = (0.5L, 0.5L)$ with respect to its initial value, namely:

$$\varepsilon_p = \frac{p_{num} - p}{p}, \tag{54}$$

where p_{num} is the numerical solution and p is the analytical solution with or without the weakly compressible correction, according to the case under consideration. The numerical outputs are characterized by Ma = 0.1 (top panel), Ma = 0.2 (middle) and Ma = 0.3 (bottom) corresponding to $\epsilon = 0.01, 0.04, 0.09$. In all the cases, the blue lines indicate the evolution obtained by using the Taylor–Green solution as initial condition, whereas the red lines

14679590, 0, Downloaded from https://onlinelibrary.wiley.com/doi/10.1111/sapm.12792 by CNR GROUP II Istituto di Scienza dell', Wiley Online Library on [15/11/2024]. See the Terms and Conditions (https://onlinelibrary.wiley.com/terms-and-conditions) on Wiley Online Library for rules of use; OA articles are governed by the applicable Creative Commons License

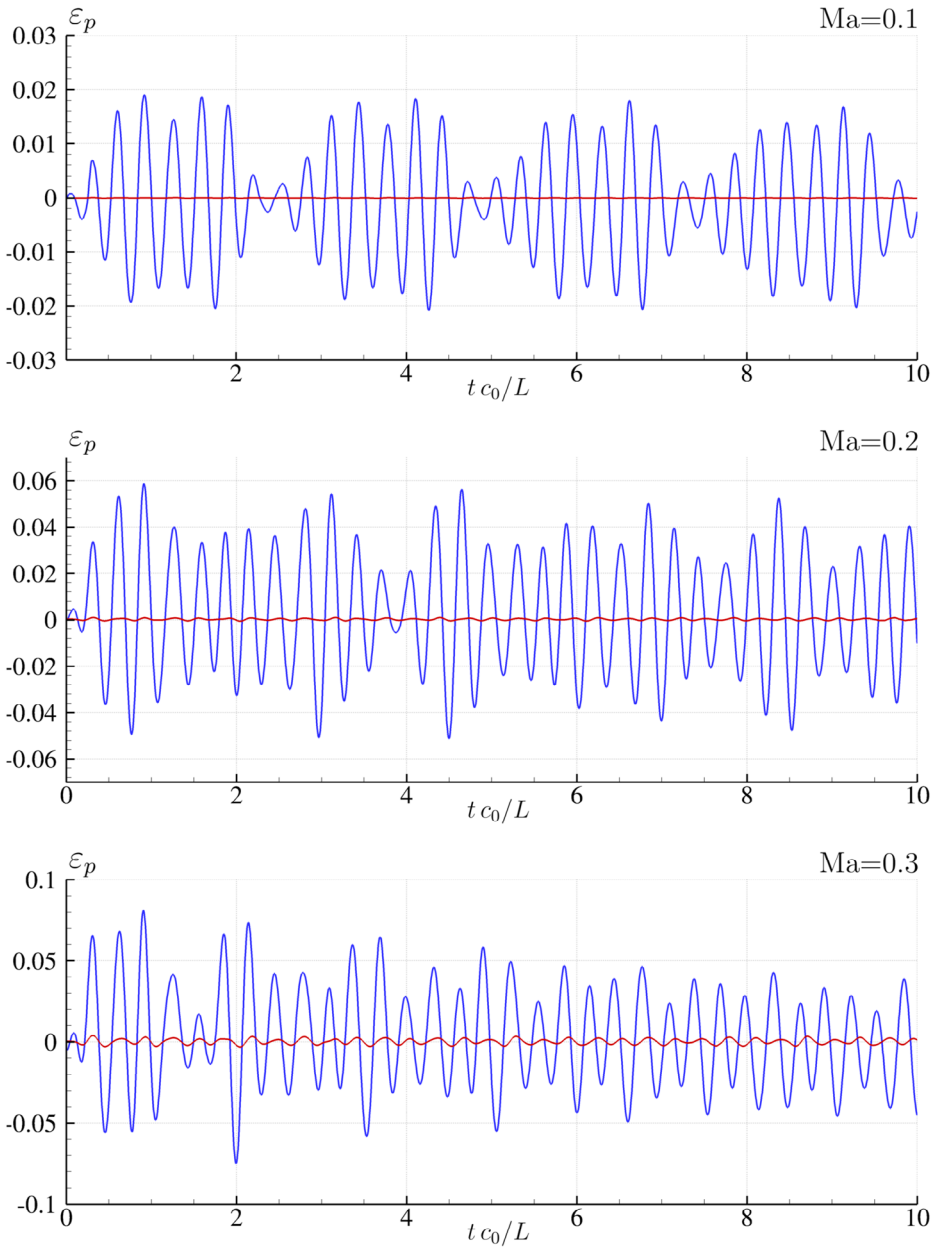

FIGURE 2 | Inviscid Taylor–Green flow simulated by means of an Eulerian meshless solver. Temporal evolution of the relative error of the pressure measured at $\boldsymbol{x}=(0.5L, 0.5L)$ using either weakly compressible initial conditions (red line) or incompressible ones (blue line) for Ma = 0.1 (top), Ma = 0.2 (middle), Ma = 0.3 (bottom). The adopted spatial resolution is $L/\Delta x = 200$.

display the same cases using the proposed weakly compressible correction. The presence of sound waves generated by the use of the incompressible solution is clear in all the numerical outputs. As expected these increase in magnitude as the ϵ increases. In particular, for Ma = 0.1, we observe a beating phenomenon similar to that reported in [4] using a finite volume scheme. Conversely, the use of the proposed correction leads to an error which is at least one order of magnitude smaller.

The numerical outputs for the viscous case are reported in Figure 3 for $\nu = 0.001$. Differently from the previous case, the time has been made dimensionless by using the reference velocity U instead of the sound velocity c_0 in order to compare in the same figure the results obtained with different Mach numbers. In the top panel of Figure 3, we display the evolution of the pressure at the origin for Ma $= 0.1, 0.2, 0.3$ as obtained by using the proposed correction as initial condition. In all the cases, the behaviour of the pressure signal is regular and little affected by acoustic noise. The same analysis is repeated in the bottom panel with the initial condition obtained from the Taylor–Green solution. Again, the latter case displays large fluctuations induced by the inconsistency of the initial conditions. As the flow evolves, these reduce in magnitude because of viscous dissipation but, despite this, persist over long times.

The last example consists in a simulation made in a Lagrangian framework which is typical of meshless particle methods like SPH solvers. Specifically, in this study the SPH model described in

14679590, 0, Downloaded from https://onlinelibrary.wiley.com/doi/10.1111/sapm.12792 by CNR GROUP II Istituto di Scienza dell', Wiley Online Library on [15/11/2024]. See the Terms and Conditions (https://onlinelibrary.wiley.com/terms-and-conditions) on Wiley Online Library for rules of use; OA articles are governed by the applicable Creative Commons License

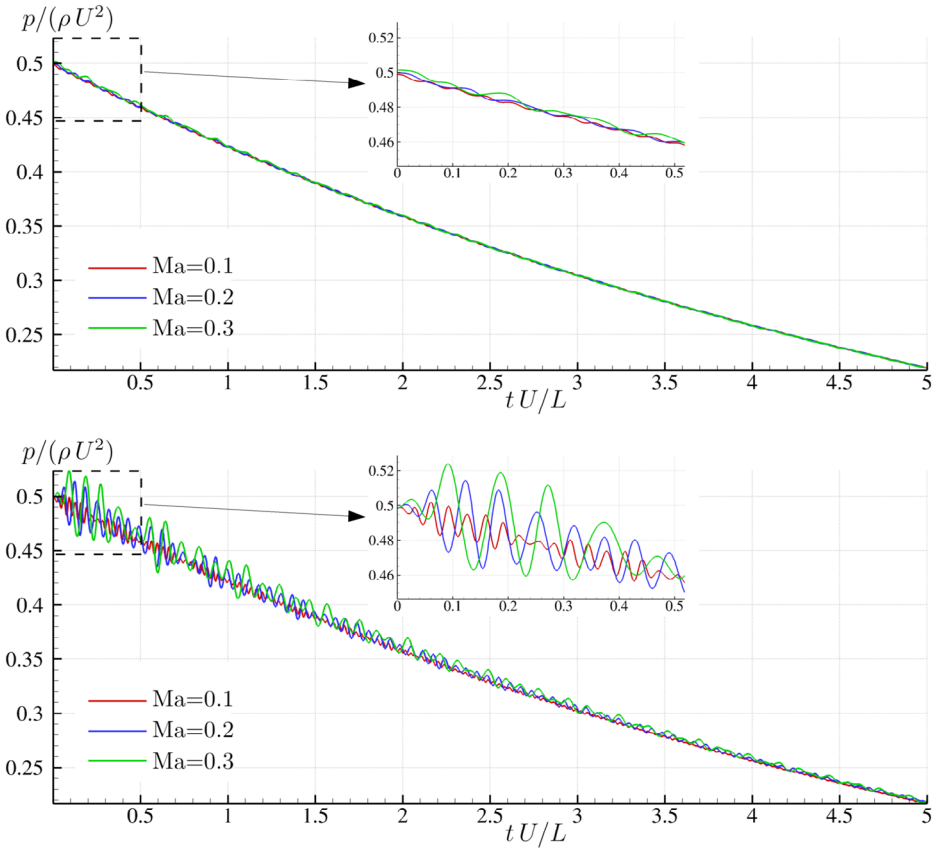

FIGURE 3 | Viscous Taylor–Green flow with $\nu = 0.001$ simulated by means of an Eulerian meshless solver. Temporal evolution of the pressure measured at $\boldsymbol{x}=(0.5L, 0.5L)$ using either weakly compressible initial conditions (top plot) or incompressible ones (bottom plot) for different Mach numbers. A zoom of the initial evolution is reported in the inset. The adopted spatial resolution is $L/\Delta x = 200$.

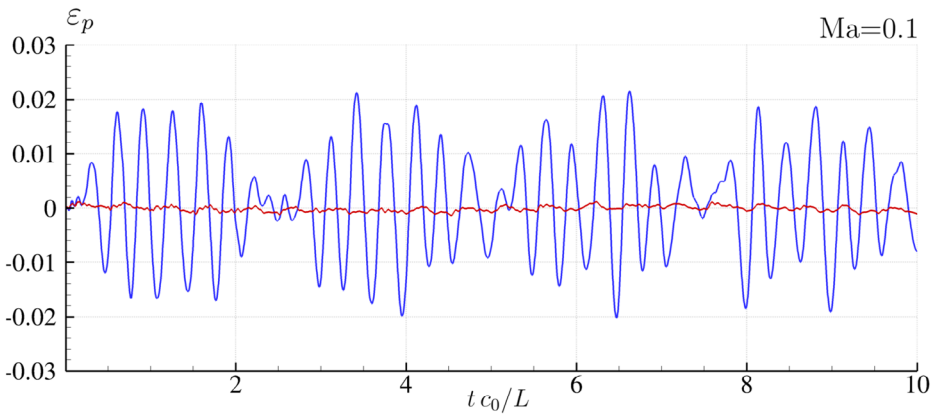

FIGURE 4 | Inviscid Taylor–Green flow simulated by means of a Lagrangian meshless solver. Temporal evolution of the relative error of the pressure measured at $\boldsymbol{x}=(0.5L, 0.5L)$ using either weakly compressible initial conditions (red line) or incompressible ones (blue line) at Ma = 0.1. The adopted spatial resolution is $L/\Delta x = 800$.

[10] is adopted. Figure 4 displays the evolution of the pressure at the origin for Ma = 0.1 with initial conditions obtained from the incompressible Taylor–Green solution (blue line) and the proposed correction (red line). Differently from the Eulerian case, for Lagrangian simulations, we needed a finer spatial resolution to be close to convergence: In this case, the adopted discretization is $L/\Delta x = 800$. In any case, the comparison with the top panel of Figure 2 displays that a similar behaviour occurs, apart from a general higher noise which is likely caused by the particle motion.

Finally, in Figure 5, a convergence study with the same test conditions as in Figure 4 is reported for initial conditions obtained from both the incompressible Taylor–Green solution (blue triangles) and the proposed correction (red squares). The comparison is performed by means of the L^1-norm of ε_p measured at the centre of the domain during the whole time span of the simulation, namely $tc_0/L = 10$. The simulations were performed starting with particle resolution $L/\Delta x = 50$ and, then, doubling the discretization up to $L/\Delta x = 800$. The observed order of

14679590, 0, Downloaded from https://onlinelibrary.wiley.com/doi/10.1111/sapm.12792 by CNR GROUP 11 Istituto di Scienza dell', Wiley Online Library on [15/11/2024]. See the Terms and Conditions (https://onlinelibrary.wiley.com/terms-and-conditions) on Wiley Online Library for rules of use; OA articles are governed by the applicable Creative Commons License

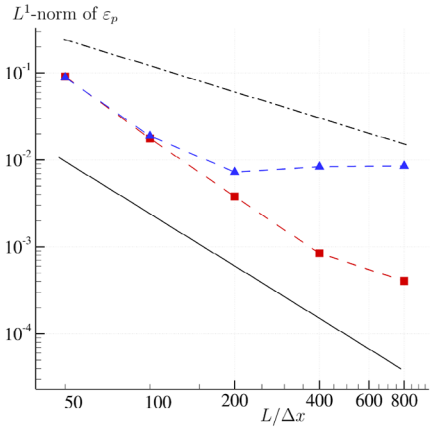

	L^1-norm of ε_p at $\boldsymbol{x}=(0.5L, 0.5L)$	
$L/\Delta x$	With correction	Without correction
50	9.075×10^{-2}	8.915×10^{-2}
100	1.765×10^{-2}	1.890×10^{-2}
200	3.793×10^{-3}	7.274×10^{-3}
400	8.454×10^{-4}	8.353×10^{-3}
800	4.034×10^{-4}	8.508×10^{-3}

FIGURE 5 | Inviscid Taylor–Green flow at Ma = 0.1 simulated by means of a Lagrangian meshless solver. Convergence of the L^1-norm of the relative error of the pressure field measured at $\boldsymbol{x}=(0.5L, 0.5L)$ for a time duration $tc_0/L=10$. Weakly compressible initial conditions are represented through red squares whereas incompressible ones with blue triangles. Left: numerical results compared to first-order (dash-dotted line) and second-order (solid line) convergence rates. Right: values of the L^1-norm obtained for both initial conditions, namely the proposed weakly compressible and the incompressible ones.

convergence for the case initialized with the proposed correction is close to 2, which is in agreement with the observations reported in [10]. Conversely, when using the incompressible Taylor–Green solution, the error reaches a plateau after $L/\Delta x = 100$ as the noise due to the initial conditions becomes predominant and does not decrease for further increases in resolution. For the reader's convenience, the values represented in Figure 5 are also reported in the table next to it.

5 | Conclusions

Assuming the fluid to be weakly compressible, we derived an approximate solution of the famous Taylor–Green solution in $\mathbb{R}^2$. This consists in a correction to the incompressible vortex solution and is valid for both viscous and inviscid fluids in two spatial dimensions. The proposed solution is expected to be a useful benchmark for those numerical solvers that rely on the weakly compressibility approximation. To this purpose, some numerical applications have been considered, proving that the proposed correction to the Taylor–Green vortex drastically reduces the acoustic noise that generates when the incompressible solution is used as an initial condition.

Acknowledgments

This research was developed within the Applied Mathematics Project Area of the Department of Engineering, ICT and Technology for Energy and Transport (DIITET) of the Italian National Research Council (CNR). The work was partially supported by the Project BIO-EMBRACE, PRIN PNRR P202298P25—CUP B53D23026860001, financed by the European Union—Next Generation EU.

Data Availability Statement

The data that support the findings of this study are available on request from the corresponding author. The data are not publicly available due to privacy or ethical restrictions.

References

1. L. Vittoz, G. Oger, M. De Leffe, and D. Le Touzé, "Comparisons of Weakly-Compressible and Truly Incompressible Approaches for Viscous Flow into a High-Order Cartesian-Grid Finite Volume Framework, " *Journal of Computational Physics: X* 1 (2019): 100015.

2. A. Bermúdez, S. Busto, M. Dumbser, J. L. Ferrín, L. Saavedra, and M. E. Vázquez-Cendón, "A Staggered Semi-Implicit Hybrid FV/FE Projection Method for Weakly Compressible Flows, " *Journal of Computational Physics* 421 (2020): 109743.

3. K. Yang and T. Aoki, "Weakly Compressible Navier-Stokes Solver Based on Evolving Pressure Projection Method for Two-Phase Flow Simulations, " *Journal of Computational Physics* 431 (2021): 110113.

4. A. Kajzer and J. Pozorski, "On the Partition Noise in Chosen Particle Weighted Methods and its Consequences for Weakly-Compressible Flow Models," *Journal of Computational Physics* 498 (2024): 112653, https://doi.org/10.1016/j.jcp.2023.112653.

5. G. Taylor, "LXXV. On the Decay of Vortices in a Viscous Fluid," *The London, Edinburgh, and Dublin Philosophical Magazine and Journal of Science* 46, no. 274 (1923): 671–674.

6. M. Brachet, "Direct Simulation of Three-Dimensional Turbulence in the Taylor–Green Vortex," *Fluid Dynamics Research* 8, no. 1-4 (1991): 1.

7. A. Di Mascio, M. Antuono, A. Colagrossi, and S. Marrone, "Smoothed Particle Hydrodynamics Method from a Large Eddy Simulation Perspective," *Physics of Fluids* 29, no. 3 (2017): 035102, https://doi.org/10.1063/1.4978274.

8. T. K. Sengupta, N. Sharma, and A. Sengupta, "Non-Linear Instability Analysis of the Two-Dimensional Navier-Stokes Equation: The Taylor-Green Vortex Problem," *Physics of Fluids* 30, no. 5 (2018): 054105, https://doi.org/10.1063/1.5024765.

9. Z. F. Meng, A. M. Zhang, P. P. Wang, F. R. Ming, and B. C. Khoo, "A Targeted Essentially Non-Oscillatory (TENO) SPH Method and Its Applications in Hydrodynamics, " *Ocean Engineering* 243 (2022): 110100.

10. J. Michel, A. Colagrossi, M. Antuono, and S. Marrone, "A Regularized High-Order Diffusive Smoothed Particle Hydrodynamics Scheme Without Tensile Instability," *Physics of Fluids* 35, no. 10 (2023): 103604, https://doi.org/10.1063/5.0165036.

11. G. I. Taylor and A. E. Green, "Mechanism of the Production of Small Eddies from Large Ones," *Proceedings of the Royal Society of London. Series A-Mathematical and Physical Sciences* 158, no. 895 (1937): 499–521.

14679590, 0, Downloaded from https://onlinelibrary.wiley.com/doi/10.1111/sapm.12792 by CNR GROUP II Istituto di Scienza dell', Wiley Online Library on [15/11/2024]. See the Terms and Conditions (https://onlinelibrary.wiley.com/terms-and-conditions) on Wiley Online Library for rules of use; OA articles are governed by the applicable Creative Commons License

12. M. Antuono, "Tri-periodic Fully Three-Dimensional Analytic Solutions for the Navier-Stokes Equations," *Journal of Fluid Mechanics* 890 (2020): A23, https://doi.org/10.1017/jfm.2020.126.

13. Wolfram Research, Inc. Mathematica, Version 14.1.; 2024. (Champaign, IL, 2024).

14. J. Michel, M. Antuono, G. Oger, S. Marrone, "Energy Balance in Quasi-Lagrangian Riemann-Based SPH Schemes, " *Computer Methods in Applied Mechanics and Engineering* 410 (2023): 116015.

15. H. Wendland, "Piecewise Polynomial, Positive Definite and Compactly Supported Radial Functions of Minimal Degree," *Advanced and Computational Mathematics* 4, no. 4 (1995): 389–396, https://doi.org/10.1007/BF02123482.

14679590, 0, Downloaded from https://onlinelibrary.wiley.com/doi/10.1111/sapm.12792 by CNR GROUP II Istituto di Scienza dell', Wiley Online Library on [15/11/2024]. See the Terms and Conditions (https://onlinelibrary.wiley.com/terms-and-conditions) on Wiley Online Library for rules of use; OA articles are governed by the applicable Creative Commons License